ACS APPLIED MATERIALS & INTERFACES

Research Article

www.acsami.org

Synthesis of Cu_2O Nanospheres Decorated with TiO_2 Nanoislands, Their Enhanced Photoactivity and Stability under Visible Light Illumination, and Their Post-illumination Catalytic Memory

Lingmei Liu,[†] Weiyi Yang,[†] Qi Li,*[,†] Shian Gao,[†] and Jian Ku Shang[†,‡]

[†]Environment Functional Materials Division, Shenyang National Laboratory for Materials Science, Institute of Metal Research, Chinese Academy of Sciences, Shenyang 110016, China

[‡]Department of Materials Science and Engineering University of Illinois at Urbana-Champaign, Urbana, Illinois 61801, United States

Supporting Information

ABSTRACT: A novel Cu_2O/TiO_2 composite photocatalyst structure of Cu_2O nanospheres decorated with TiO_2 nanoislands were synthesized by a facile hydrolyzation reaction followed by a solvent-thermal process. In this Cu_2O/TiO_2 composite photocatalyst, Cu_2O served as the main visible light absorber, while TiO_2 nanoislands formed heterojunctions of good contact with Cu_2O, beneficial to the photoexcited electron transfer between them. Their band structure match and inner electrostatic field from the *p*–*n* heterojunction both favored the transfer of photoexcited electrons from Cu_2O to TiO_2, which effectively separated the electron–hole pairs. Photogenerated holes on Cu_2O could react with water or organic pollutants/microorganisms in water to avoid accumulation on Cu_2O because of the partial TiO_2 nanoislands coverage, which enhanced their stability during the photocatalysis process. Their superior photocatalytic performance under visible light illumination was demonstrated in both the degradation of methyl orange and the disinfection of *Escherichia coli* bacteria. An interesting post-illumination catalytic memory was also observed for this composite photocatalyst as demonstrated in the disinfection of *Escherichia coli* bacteria in the dark after the visible light was shut off, which could be attributed to the transfer of photoexcited electrons from Cu_2O to TiO_2 and their trapping on TiO_2 under visible light illumination, and their release in the dark after the visible light was shut off.

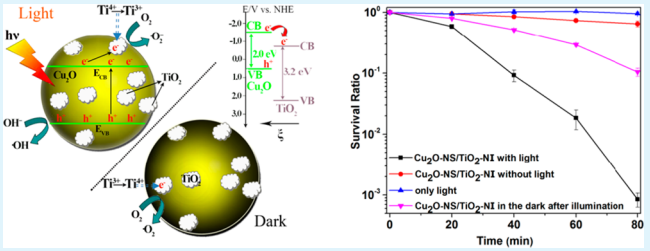

KEYWORDS: *Cu_2O/TiO_2 composite photocatalyst, p–n heterojunction, visible-light-activated photocatalysis, enhanced performance/stability, catalytic memory*

1. INTRODUCTION

Over the past a few decades, semiconductor-based photocatalysts have attracted research attentions for both solar energy conversion, and environmental applications. Among various photocatalysts, *p*-type Cu_2O with a direct-band of 2.0 eV has been widely examined by many groups on applications for water splitting, solar cell, gas sensor, and so on.[1−4] While the narrow band gap contributes to its effective utilization of solar energy, its strong adsorption of molecular oxygen could scavenge photoelectrons, minimizing the electron–hole pair recombination on its surface.[5,6] Furthermore, Cu_2O has a low toxicity, is inexpensive, and has a good environmental acceptability, which makes it a potential alternative to other photocatalysts, such as TiO_2, for the photocatalytic degradation of organic contaminations.[7−9]

However, the rapid recombination of photoinduced electron–hole pairs and the instability of Cu_2O under light illumination seriously limit its photocatalytic performance.[10,11] It had been reported that the valence and conduction bands of Cu_2O are higher than those of TiO_2, which thermo-dynamically favors the transfer of excited electrons and holes between them and could subsequently enhance the separation of charge carriers to decrease their recombination.[12−14] Most previous studies of Cu_2O/TiO_2 heterojuntion photocatalysts were based on TiO_2 and a small amount of Cu_2O deposited onto TiO_2 surface to provide visible light absorption.[15,16] Some other researchers synthesized Cu_2O/TiO_2 core–shell structure or TiO_2/Cu_2O layered film structure to protect Cu_2O from corrosion.[17,18] However, the main visible light absorber in this composite photocatalyst system was the narrow-band-gap semiconductor Cu_2O. Thus, photocatalysts based on TiO_2 with just a small amount of Cu_2O could not achieve high photoactivity under visible light illumination because of the small portion of light absorber in this composite photocatalyst system. For Cu_2O/TiO_2 core-shell structure or TiO_2/Cu_2O layered film structure, although the interface area of heterojuntions was largely increased, the Cu_2O core or the underlying Cu_2O film could not directly contact with water or

Received: January 8, 2014
Accepted: March 27, 2014
Published: March 27, 2014

   dx.doi.org/10.1021/am500131b | ACS Appl. Mater. Interfaces 2014, 6, 5629−5639

pollutants in water and the holes accumulation will occur in Cu_2O which may cause further photocorrosion on Cu_2O.

In this work, a novel Cu_2O/TiO_2 composite photocatalyst structure of Cu_2O nanospheres (Cu_2O-NS) decorated with TiO_2 nanoislands (TiO_2-NI) was synthesized successfully. In this Cu_2O/TiO_2 composite photocatalyst, Cu_2O nanospheres served as the main component for light absorption so it demonstrated excellent absorption capability in the visible light region. TiO_2 nanoislands formed heterojunctions of good contact with Cu_2O nanospheres, beneficial to the photoexcited electron transfer between them. The close match of their band structures and the inner electrostatic field from the $p-n$ heterojunction favored the transfer of photoexcited electrons from Cu_2O to TiO_2, which effectively separated the electron–hole pairs and subsequently enhanced their photocatalytic performance under visible light illumination as demonstrated in the photocatalytic degradation of methyl orange (MO) and disinfection of *Escherichia coli* (*E. coli*) bacteria. The partial coverage of TiO_2 nanoislands made it possible for photogenerated holes to react with water to produce $^{\bullet}OH$s or directly react with organic pollutants/microorganisms in water to avoid the accumulation of holes on Cu_2O. Without the accumulated holes, the photochemical stability of Cu_2O was enhanced during the photocatalysis process. Furthermore, a post-illumination catalytic memory was also observed for this composite photocatalyst, which demonstrated a disinfection effect on *E. coli* bacteria in the dark after the visible light was shut off. This interesting post-illumination catalytic memory could be attributed to the transfer of photoexcited electrons from Cu_2O to TiO_2 under visible light illumination, which could by trapped by TiO_2 nanoislands and then be released in the dark to produce radicals for the demonstrated catalytic memory.

2. EXPERIMENTAL SECTION

2.1. Chemicals and Materials. Copper(II) chloride dihydrate ($CuCl_2{\cdot}2H_2O$, 99%, Sinopharm Chemical Reagent Co., Ltd., Shanghai, P. R. China) was used as the Cu source, polyvinylpyrrolidon (PVP k30, Sinopharm Chemical Reagent Co., Ltd., Shanghai, P. R. China) was used as the surfactant, sodium hydroxide (NaOH, 96%, Sinopharm Chemical Reagent Co., Ltd., Shanghai, P. R. China) was used as the precipitation reagent, and L-ascorbic acid (99.7%, Kemiou Chemicals Co. Ltd., Tianjin, P. R. China) was used as the reducing agent in the synthesis of Cu_2O nanospheres, respectively. Deionized water (DI) was used as the solvent in this process. Tetrabutyltitanate (TBT, 98%, Tianjin baishi Reagent Plant, Tianjin, P. R. China) was used as the Ti source and ethyl alcohol (EtOH, 99.7%, Beijing Yili Fine Chemicals Co. Ltd., Beijing, P. R. China) was used as the solvent in the solvent–thermal process. Commercially available Degussa P25 TiO_2 nanoparticles (Evonik Industries, Germany) were used for the comparison with Cu_2O nanospheres and Cu_2O-NS/TiO_2–NI on their visible-light photocatalytic performance.

2.2. Synthesis of Cu_2O Nanospheres. The Cu_2O nanospheres were synthesized according to a reported process.[19] In a typical experiment, 0.4 g PVP was first dissolved in 200 mL of deionized water, and 10 mL of 0.04 M $CuCl_2{\cdot}2H_2O$ solution was added into the PVP solution. Then, 3.6 mL of 0.4 M NaOH was added drop wise (1 drop/s) into the above mixture solution with continual stirring. Finally, 4 mL of 0.2 M L-ascorbic acid was added dropwise and the solution was further stirred for 5 min before being centrifuged at 9500 rpm for 5 min. The obtained yellow precipitates were washed with excessive deionized (DI) water and ethanol for several times to remove unreacted chemicals and PVP surfactants.

2.3. Preparation of Cu_2O Nanospheres Decorated with TiO_2 Nanoislands. The obtained Cu_2O was immediately dispersed in 10 mL of ethanol with the aid of ultrasonication for 10 min. Then, 0.2 mL of 0.1 M Tetrabutyloxytitanate (TBT) was slowly dropped into the Cu_2O suspension and stirred at 0 °C for 1 h. After it was thoroughly mixed, 1 mL of water/ethanol solution in a volume ratio of 1:4 was added drop wise into the mixture under vigorous stirring for another hour. Finally, the suspension was diluted with 15 mL of ethanol and was transferred into a 40 mL Teflon-lined stainless steel autoclave, and heated at 180 °C for 12 h in an oven. After the reaction, the products were collected, went through several rinse-centrifugation cycles with DI water and ethanol separately, and then dried at 60 °C for 10 h in a vacuum oven. Bare TiO_2 was prepared via the same hydrolyzation and solvent–thermal process, while the same solvent-thermal process was also conducted on obtained Cu_2O nanospheres. Their physical mixture was used as a reference material for the photocatalytic testing.

2.4. Material Characterization. The crystal structures of the as-prepared samples were analyzed by X-ray diffraction (XRD) on a D/MAX-2004 X-ray powder diffractometer (Rigaku Corporation, Tokyo, Japan) with Ni-filtered Cu Kα (λ = 1.54178 Å) radiation at 56 kV and 182 mA. The morphologies of the as-prepared samples were observed by the field emission scanning electron microscopy (FESEM) and the transmission electron microscopy (TEM). FESEM observations were conducted by a ZEISS SUPRA35 SEM (ZEISS, Germany). TEM observations were conducted on a JEOL 2100 TEM (JEOL Ltd., Tokyo, Japan) operated at 200 kV with point-to-point resolution of 0.28 nm, and TEM samples were prepared by dispersing a thin film of these powder samples on Ni grids. A Tecnai G2 F30 transmission electron microscope (FEI, Acht, the Netherlands) equipped with high-angle-angular-dark-field (HAADF) and x-ray dispersive spectroscopy (EDS) systems was used to investigate the composition and structure of samples. X-ray photoelectron spectroscopy (XPS) measurements were conducted using an ESCALAB 250 X-ray photoelectron spectrometer (Thermo Fisher Scientific Inc., Waltham, MA, U. S. A.) with an Al K anode (1486.6 eV photon energy, 300 W). The UV–vis spectra of samples were measured on a UV-2550 spectrophotometer (Shimadzu Corporation, Kyoto, Japan). The surface photovoltage spectra (SPS) of samples were measured with a home-built apparatus that had been described in details elsewhere.[20]

2.5. Photocatalytic Degradation of Methyl Orange under Visible Light Illumination. Methyl orange was used as a model organic pollutant to evaluate the photocatalytic activity of samples under visible light illumination. First, 0.03 g of photocatalyst was dispersed in 75 mL of DI water by ultrasonication for 10 min, followed by adding 75 mL of 60 mg/L aqueous MO solution. Thus, the initial concentration of MO in the solution was 30 mg/L, and a fixed concentration of 0.2 mg photocatalyst/mL solution was used. A 300 W xenon lamp (PLS-SXE300, Beijing PerfectLight Technology Co., Ltd., Beijing, P. R. China) was used as the light source, which has a glass filter to provide zero light intensity below 400 nm. The light intensity striking the MO solution was at ~23 mW/cm^2, as measured by a FZ-A optical Radiometer (Photoelectric Instrument Factory of Beijing Norman University, Beijing, P. R. China). At each time interval, photocatalysts were separated by centrifugation at 10 500 rpm for 5 min, and the light absorption of the clear solution was measured by the UV-2550 spectrophotometer. P25 TiO_2 nanoparticles and bare Cu_2O nanospheres after the solvent–thermal process were also used in the photocatalytic degradation of MO experiments for comparison purpose under the same experimental conditions. For the cycle performance tests, the recovered photocatalysts after the degradation experiment were dried in a vacuum oven for 10 h before their reuse for the next run. All analyses were in triplicate.

2.6. Photocatalytic Disinfection of Bacteria *Escherichia coli* (*E. coli*) under Visible Light Illumination. Wild-type *E. coli* AN 387 (ATCC 15597, the American Type Culture Collection, Manasss, VA, USA) were used for photocatalytic disinfection experiment. After overnight culture, cells were diluted to a cell suspension (~10^7 cfu/mL) in buffer solution (0.05 M KH_2PO_4 and 0.05 M K_2HPO_4, pH 7.0) prior to the use for photocatalytic disinfection experiments. All solid or liquid materials had been autoclaved for 30 min at 121 °C before use. The same visible light source was used as in the photocatalytic degradation of MO. In the photocatalytic disinfection of *E. coli* bacteria experiment, aliquot of 10 mL *E. coli* cell suspension was

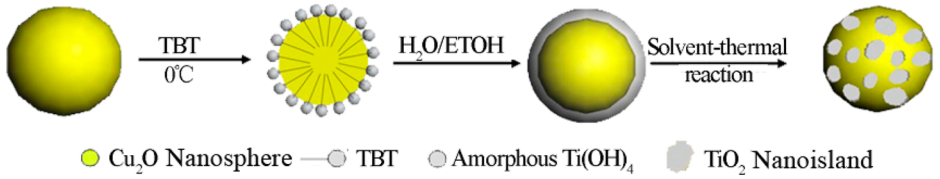

Figure 1. Schematic illustration of the synthesis process of Cu_2O nanospheres decorated with TiO_2 nanoislands.

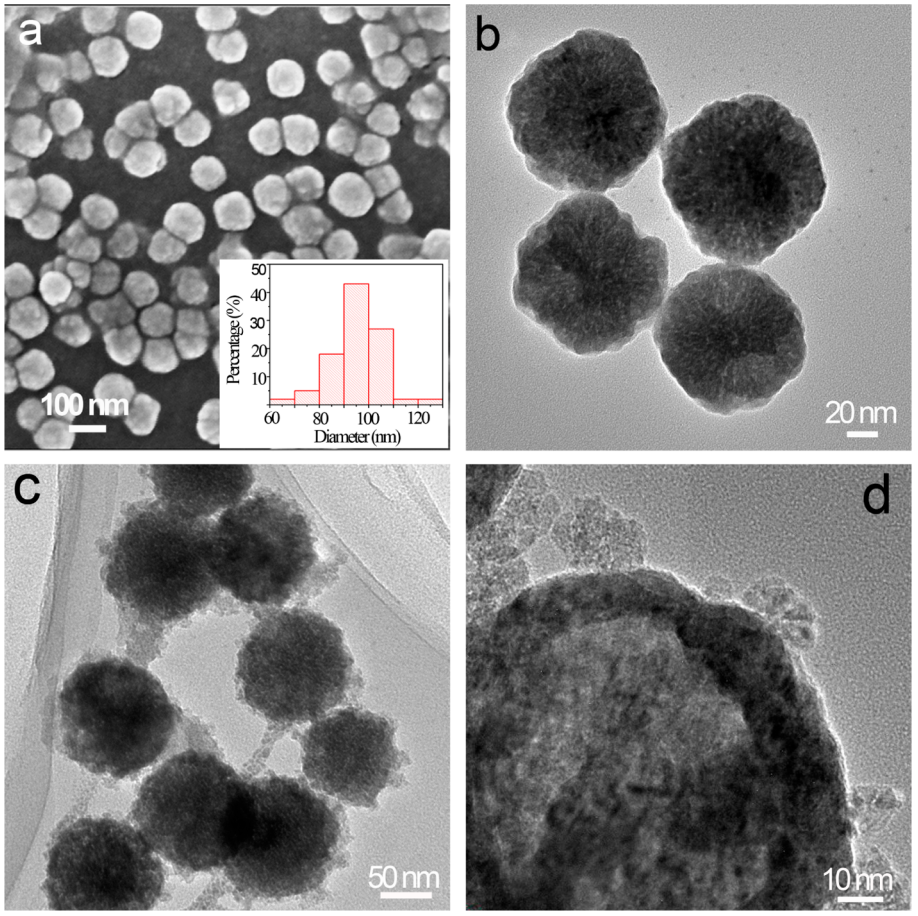

Figure 2. (a) SEM image (inset, nanosphere size distribution) and (b) TEM image of the as-prepared Cu_2O nanospheres. (c) TEM image of Cu_2O nanospheres covered with amorphous $Ti(OH)_4$ layer. (d) TEM image of Cu_2O nanospheres decorated with TiO_2 nanoislands after the solvent thermal reaction.

pipetted onto a sterile 50 × 10 mm petri dish with photocatalytic powder samples placed at the bottom. A fixed concentration of ~1 mg photocatalyst/mL *E. coli* solution was used in this experiment. At regular time intervals, 100 μL of aliquots of the powder-treated cell suspensions were withdrawn in sequence. After appropriate dilutions in buffer solution, aliquot of 100 μL was spread onto an agar medium plate and incubated at 37 °C for 15 h. The number of viable cells in terms of colony-forming units was counted. Tests were also performed in the dark in the presence of the photocatalyst for comparison. Analyses were in triplicate, and control runs were carried out each time under the same experiment conditions, but without any photocatalytic materials.

2.7. Catalytic Memory Disinfection of Bacteria *Escherichia coli* (*E. coli*) in the Dark. For *E. coli* bacteria disinfection under dark environment, Cu_2O-NS/TiO_2-NI sample was firstly illuminated by the same lamp for ~3 h. Then, the lamp was shut off and they were used to conduct disinfection experiment in the dark over fresh *E. coli* cell suspensions (~10^7 cfu/mL) either immediately or after being kept in dark for 8 h. All experimental conditions were the same as that for the photocatalytic disinfection of *E. coli* bacteria, but without the visible light illumination.

3. RESULTS AND DISCUSSION

3.1. Synthesis of Cu_2O Nanospheres Decorated with TiO_2 Nanoislands. Figure 1 schematically demonstrates the synthesis process of these Cu_2O nanospheres decorated with TiO_2 nanoislands. In the first step, Cu_2O nanospheres were synthesized with a simple precipitation process during which ascorbic acid was used as the reductant to reduce Cu^{2+} to Cu^+ to form Cu_2O nanoparticles. Figure 2a and 2b shows the SEM and TEM images of the as-prepared Cu_2O nanospheres, respectively. They were largely spherical in shape, composed of nanocrystallites of ~10−30 nm and had an average size of ~100 nm. In the second step, a good adsorption of TBT molecules onto the surface of Cu_2O nanospheres was crucial for the subsequent formation of hererojunctions. In the third step, a water/ethanol solution (molar ratio of 1:4) was added drop wise into the mixture under vigorous stirring, during which the adsorbed TBT molecules underwent a hydrolysis reaction with water molecules and formed a layer of $Ti(OH)_4$ on the surface

dx.doi.org/10.1021/am500131b | ACS Appl. Mater. Interfaces 2014, 6, 5629−5639

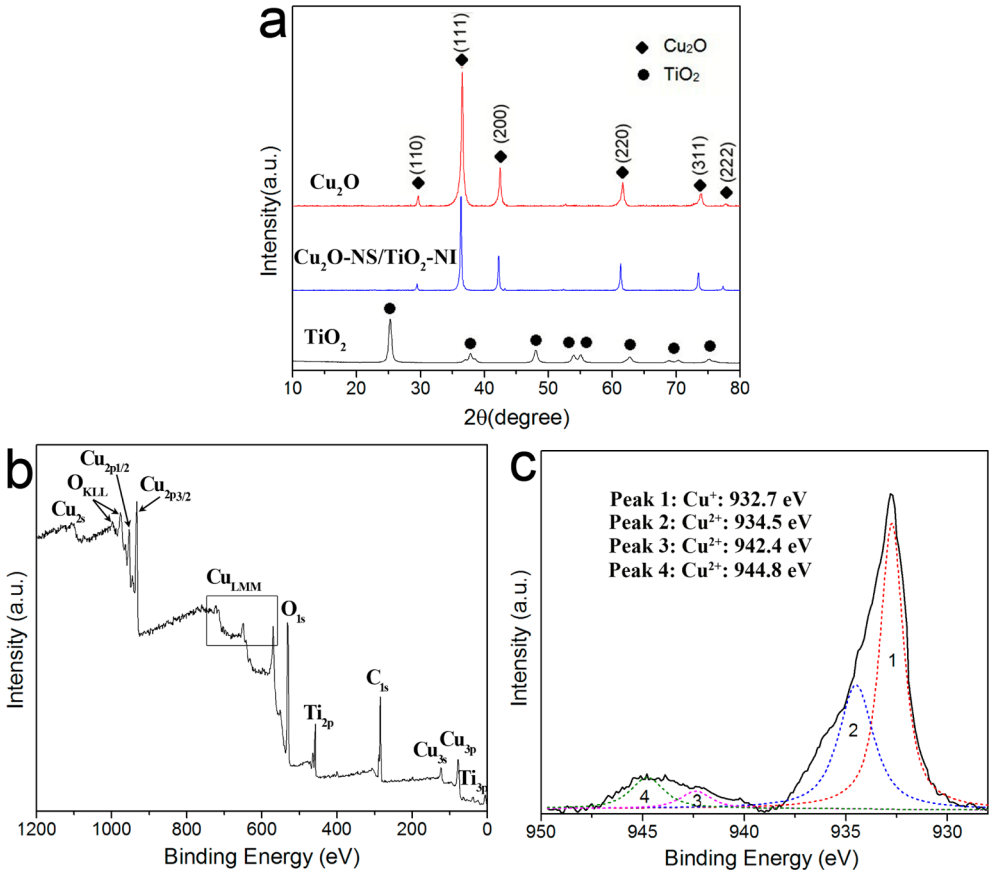

Figure 3. (a) X-ray diffraction patterns of as-synthesized Cu_2O nanospheres, Cu_2O-NS/TiO_2-NI, and anatase TiO_2 nanoparticles. (b) XPS survey spectrum of Cu_2O-NS/TiO_2-NI. (c) The high resolution XPS scans over Cu $2p_{3/2}$ peak.

of these Cu_2O nanospheres. Figure 2c shows the TEM image of samples after the third step, which clearly demonstrated that a rough shell covered the Cu_2O nanosphere core. In this process, the modulation of reaction temperature and water amount/concentration in the water/ethanol solution is critical to obtain a relatively uniform shell. An ice water bath and the use of mixture of water/ethanol with proper ratio could slow down the hydrolysis reaction of TBT for a better control of the shell formation. In the final step, a solvent-thermal process was adopted with ethanol as the solvent to dehydrate $Ti(OH)_4$ to TiO_2 and crystallize it. Figure 2d shows the TEM observation of obtained samples after the final step, which clearly demonstrated that the rough shell (as in Figure 2c) covered the Cu_2O nanosphere core disappeared and nanoislands occurred on the surface of these Cu_2O nanospheres, which were composed of clusters of TiO_2 nanoparticles. During the $Ti(OH)_4$ dehydration process, the amorphous $Ti(OH)_4$ layer largely shrank to form TiO_2, which broke the continuous layer and formed nanoisland structures.

3.2. Crystal Structure and Chemical Composition of Cu_2O Nanospheres Decorated with TiO_2 Nanoislands. Figure 3a shows the X-ray diffraction pattern of as-synthesized Cu_2O nanospheres, anatase TiO_2 nanoparticles, and Cu_2O-NS/TiO_2-NI. For both Cu_2O nanospheres and Cu_2O-NS/TiO_2-NI, no diffraction peaks of CuO or Cu could be detected, and all diffraction peaks belonged to the face-centered cubic Cu_2O phase (PDF Card No. 05-0667). The crystallite size of Cu_2O could be obtained from the strongest diffraction peak (at $2\theta \approx 36.4°$ for fcc phase) by the Scherrer's formula[21]

$$D = 0.9\lambda/\beta \cos\theta \quad (1)$$

where λ is the average wavelength of the X-ray radiation, β is the line-width at half-maximum peak position, and θ is the XRD peak. The average crystallite size of as-synthesized Cu_2O nanospheres was determined at ~21.6 nm, while the average crystallite size of Cu_2O-NS/TiO_2-NI was determined at ~30.2 nm. Interestingly, no peaks of anatase TiO_2 could be observed for Cu_2O-NS/TiO_2-NI sample, which might be attributed to the low content of TiO_2 in this composite photocatalyst system.

Figure 3b shows XPS survey spectrum of Cu_2O-NS/TiO_2-NI, which demonstrated clearly the existence of Ti, O, and Cu in the sample. Due to the widespread presence of carbon in the environment, C 1s peak could also be observed clearly in the XPS survey spectrum. Figure 3c shows the high resolution XPS scans over Cu $2p_{3/2}$ peak. The main peak at 932.7 eV was known as the characteristic of Cu^+,[22,23] while the shake-up satellite peaks on the higher binding energy side, 934.5, 942.4, and 944.8 eV, indicated the presence of an unfilled Cu 3d shell and thus confirmed the existence of Cu^{2+} on the sample surface.[24,25] As a surface characterization technique, XPS could determine the surface composition ratio within a very shallow depth. This observation and XRD analysis result suggested that a small portion of Cu_2O on the nanoparticle surface was oxidized to CuO during the sample drying and handling under normal ambient condition, and the amount of CuO was too low to be detected by XRD. This phenomenon had been reported by many researchers on the synthesis of Cu_2O nanoparticles, and it had been found that a small amount of

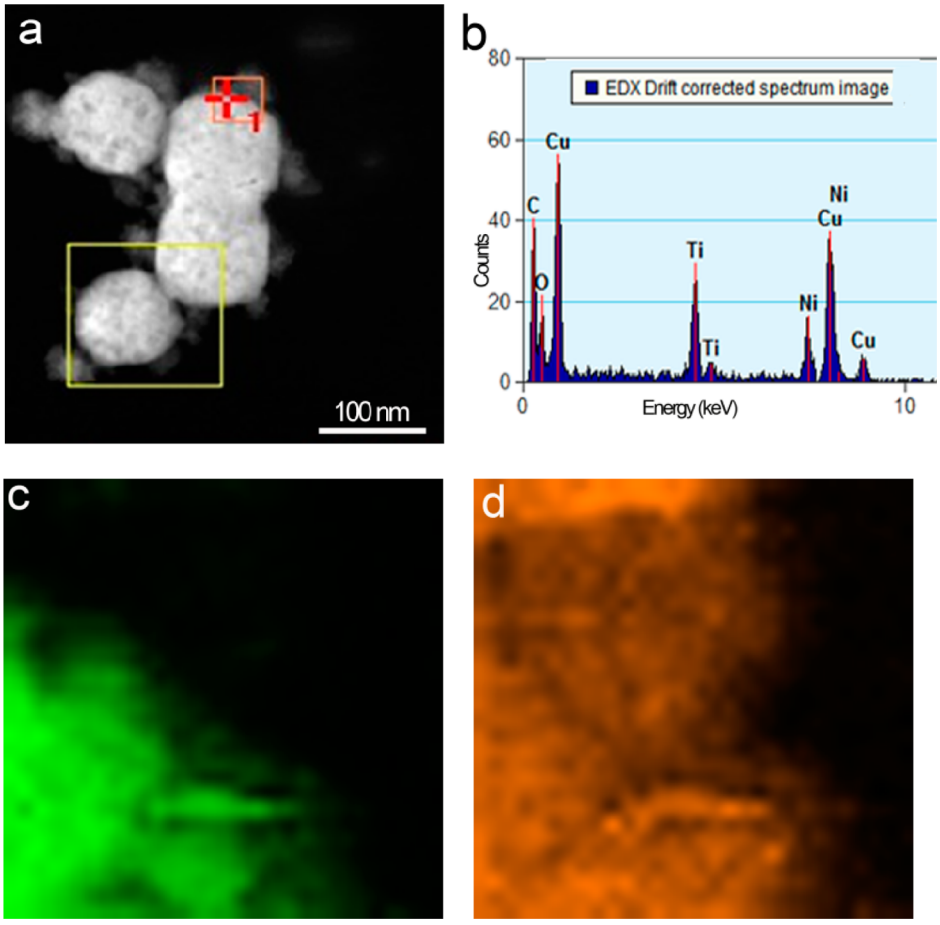

Figure 4. (a) STEM image of Cu_2O-NS/TiO_2-NI photocatalysts. (b) EDS analysis result on the place defined by the red cross in panel a. (c and d) Distribution map of Cu and Ti elements in the area defined by the small red square in panel a, respectively.

CuO on Cu_2O nanoparticle surface could actually enhance its stability.[24,26]

3.3. Formation of Heterojunction between Cu_2O and TiO_2. To further verify the existence of TiO_2, Cu_2O nanospheres decorated with TiO_2 nanoislands were analyzed with the energy dispersive X-ray analysis (EDS). Figure 4a shows the STEM image of several Cu_2O nanospheres decorated with TiO_2 nanoislands, which demonstrated clearly that nanoislands existed on these nanospheres. Figure 4b shows the EDS analysis result on the place defined by the red cross in Figure 4a, which verified the existence of Cu, Ti, and O in this area. The signals of Ni and C were also present, which came from the Ni grid for the sample support and the wide spread presence of carbon in the environment, respectively. Figure 4c and 4d shows the distribution map of Cu and Ti elements in the area defined by the small red square in Figure4a, respectively. Figure 4c demonstrated that Cu element was only found in the large nanospheres and its presence was not found in the nanoisland area, while Figure 4d demonstrated that Ti element could be found in the nanoisland area and on the large nanosphere surface. The element distribution map analysis verified that TiO_2 existed as nanoislands on the surface of Cu_2O nanospheres.

Figure 5a shows the representative HRTEM image of the Cu_2O/TiO_2 interface area on these Cu_2O-NS/TiO_2-NI photocatalysts. The HRTEM image of the TiO_2 nanoisland area verified its highly crystallized structure (region I). One set of lattice planes could be clearly observed with the *d*-spacing at

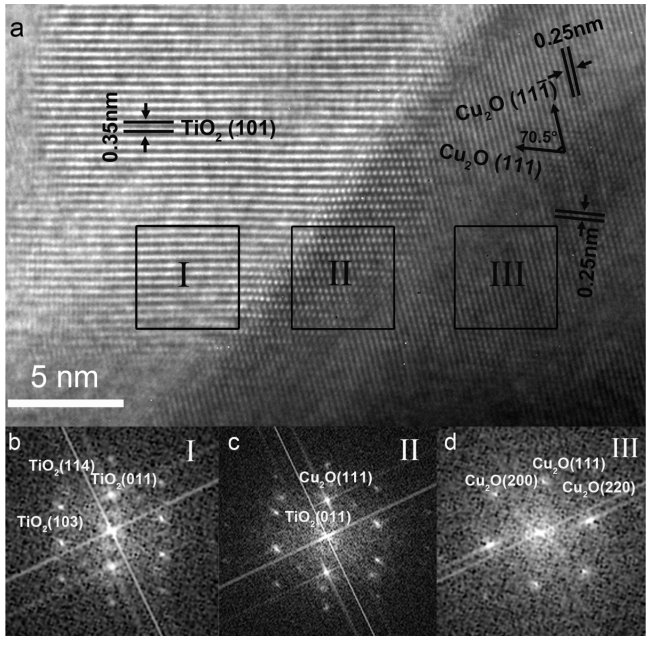

Figure 5. (a) HRTEM image of the Cu_2O/TiO_2 interface area on these Cu_2O-NS/TiO_2–NI photocatalysts. (b–d) Corresponding fast Fourier transformation (FFT) patterns of regions I, II, and III in panel a, respectively.

dx.doi.org/10.1021/am500131b | ACS Appl. Mater. Interfaces 2014, 6, 5629–5639

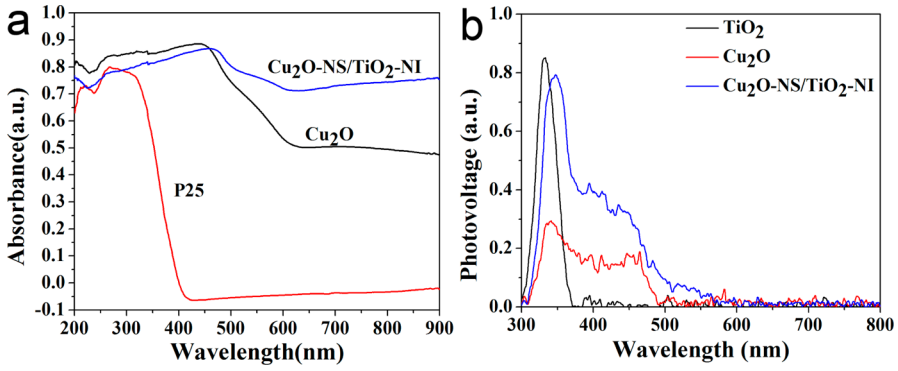

Figure 6. (a) UV−vis light absorbance spectrum of Cu_2O-NS/TiO_2-NI photocatalysts, compared with that of the as-synthesized Cu_2O nanospheres and Degussa P25 TiO_2 nanoparticles. (b) Surface photovoltage spectrum of Cu_2O-NS/TiO_2-NI photocatalysts, compared with that of the as-synthesized Cu_2O nanospheres and anatase TiO_2 nanoparticles.

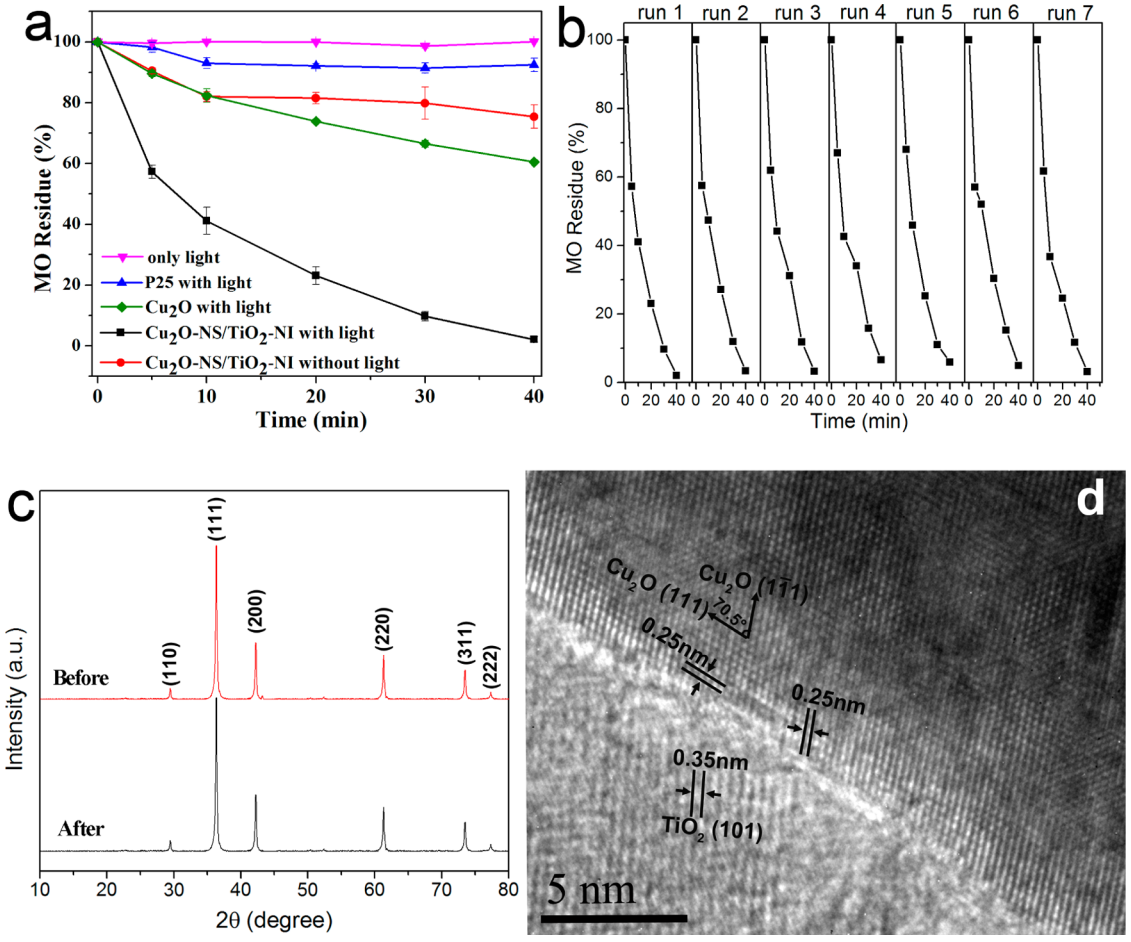

Figure 7. (a) Residue MO percentage vs treatment time in treated MO solutions under different treatment conditions. (b) The photocatalytic degradation of MO by Cu_2O-NS/TiO_2-NI photocatalysts under visible light illumination for seven runs. (c) XRD patterns and (d) HRTEM of Cu_2O-NS/TiO_2-NI photocatalysts after seven times photocatalytic degradation of MO.

~0.35 nm, corresponding to the (101) plane of the anatase TiO_2 phase. The HRTEM image of the Cu_2O nanospheres also verified its highly crystallized structure (region III). Two sets of lattice planes could be clearly observed with the *d*-spacing at ~0.25 and ~0.25 nm, respectively, and their separation angle was ~70.5°, corresponding to the (111) and (11$\bar{1}$) planes of the fcc Cu_2O phase. The well-crystallized nature of both Cu_2O and TiO_2 are beneficial to a good photocatalytic performance because of the lack of crystal defects. The Cu_2O/TiO_2 interface area (region II) was also well-crystallized, and a gradual transition of the fcc Cu_2O phase to the anatase TiO_2 phase could be observed. This observation indicated that these TiO_2 nanoislands grew on Cu_2O nanoparticles through our synthesis approach and formed heterojunctions with good contact between Cu_2O and TiO_2, which was beneficial to the photoexcited electron transfer between them. Figure 5b−5d shows the corresponding fast Fourier transformation (FFT) patterns of regions I−III in Figure 5a, respectively. Their FFT patterns further verified that region I consisted of well-crystallized anatase TiO_2, region III consisted of well-crystal-

dx.doi.org/10.1021/am500131b | ACS Appl. Mater. Interfaces 2014, 6, 5629−5639

lized fcc Cu_2O, and region II, the heterojunction interface, consisted of both TiO_2 and Cu_2O with good crystallization.

3.4. Optical Properties and SPS Analysis Results of Cu_2O Nanospheres Decorated with TiO_2 Nanoislands. The optical properties of these Cu_2O-NS/TiO_2-NI photocatalysts were investigated by measuring their diffuse reflectance spectrum. From the reflectance data, optical absorbance can be approximated by the Kubelka−Munk function, as given by eq 2

$$F(R) = \frac{(1-R)^2}{2R} \quad (2)$$

where R is the diffuse reflectance.[27] Figure 6a shows the light absorbance (in term of Kubelka−Munk equivalent absorbance units) of Cu_2O-NS/TiO_2-NI, compared with the light absorbance of the as-synthesized Cu_2O nanospheres and the commercially available Degussa P25 TiO_2 nanoparticles. Degussa P25 nanoparticles are widely used in the photocatalytic research as a model TiO_2 with high photocatalytic performance, and they demonstrated the characteristic spectrum with the fundamental absorbance stopping edge at ∼400 nm. Cu_2O nanospheres, however, demonstrated a much enhanced light absorption in the visible light region. Their absorbance stopping edge was found at ∼600 nm, which was in accordance with the reported band gap of Cu_2O at ∼2.0 eV.[28] After being partially covered with TiO_2 nanoislands, an even better visible light absorbance was observed on Cu_2O nanospheres. This observation may be attributed to the Cu_2O crystallite size increase during the solvent−thermal reaction process and the scattering of visible light from TiO_2 nanoislands which was superimposed on the absorption of these Cu_2O-NS/TiO_2-NI photocatalysts.

It is well known that photocatalysts may not demonstrate photocatalytic activity even with light absorption because of the loss of charge carriers becaue of their recombination. Thus, the detection of charge carriers that transfer to the surface of photocatalysts could provide more accurate working light range estimation for their photocatalytic response. The surface photovoltage spectrum (SPS) measurements were conducted on pure anatase TiO_2 nanoparticles, as-synthesized Cu_2O nanospheres, and Cu_2O-NS/TiO_2-NI photocatalysts (see Figure 6b), which is a powerful tool for investigating the photoinduced carrier separation and transfer behavior.[29,30] The illumination-induced changes in the surface voltage of pure anatase TiO_2 were limited within the UV light region, which was in accordance with its light absorption capability. For as-synthesized Cu_2O nanospheres, their illumination-induced changes in the surface voltage were extended to the visible light region. It could be found that the stopping edge was ∼500 nm, smaller than their light absorbance stopping edge (∼600 nm), and their illumination-induced changes within the UV light region were smaller than that of pure anatase TiO_2. These observation results may be attributed to the massive charge carrier recombination problem in Cu_2O, which had been reported in literature.[12] When decorated with TiO_2 nanoislands, however, much larger illumination-induced changes were demonstrated by these Cu_2O nanospheres. The stopping edge increased to ∼600 nm, and their illumination-induced changes from the UV light region to visible light region were larger than that of pure anatase TiO_2 and as-synthesized Cu_2O nanospheres. This observation suggested that these Cu_2O-NS/TiO_2-NI photocatalysts had largely enhanced charge separation efficiency, which could increase the lifetime of charge carriers and subsequently show a better photocatalytic performance under visible light illumination.

3.5. Photocatalytic Degradation of Methyl Orange under Visible Light Illumination. The photocatalytic activities of these Cu_2O-NS/TiO_2-NI photocatalysts were demonstrated by their degradation effect on a model organic contaminant, methyl orange, under visible light illumination. Figure 7a summaries the residue MO concentration versus treatment time under different conditions. When there was no photocatalyst presence, MO solution kept most of its initial concentration under visible light illumination, and no obvious degradation was observed. Under visible light illumination, Degussa P25 TiO_2 nanoparticles displayed a weak MO removal capability. After 40 min treatment, the residual MO concentration was still ∼90%, which could be attributed to its weak photocatalytic activity under visible light illumination from their relatively wide band gap (∼3.0 eV). The bare Cu_2O nanospheres after the solvent-thermal process demonstrated a better photocatalytic degradation effect on MO under visible light illumination. After 40 min treatment, the residual MO concentration dropped to ∼60%. The physical mixture of bare TiO_2 and Cu_2O was also used for the photocatalytic MO degradation. It showed a very similar photocatalytic performance as that of bare Cu_2O nanospheres after the solvent-thermal process (not shown in Figure 7a). This observation is easy to understand because the content of TiO_2 was very low in the mixture, and the two components could not contact with each other well to form heterojuntions. Cu_2O-NS/TiO_2-NI photocatalysts demonstrated the best photocatalytic degradation on MO under visible light illumination. When there was no light illumination, the decrease of MO concentration was due to its adsorption on these Cu_2O-NS/TiO_2-NI photocatalysts.[31] After about 10 min adsorption, the residual MO concentration reached a plateau at ∼80%. With visible light illumination, the residual MO concentration continued to decrease with the increase of the treatment time. After 40 min treatment, the residual MO concentration dropped to approximately just 3%, representing a nearly complete photocatalytic degradation.

The slope of the MO degradation curve in Figure 7a represents the MO degradation rate at certain treatment time. The photocatalytic activity enhancement could be further demonstrated quantitatively by the initial MO degradation rates for different photocatalysts with the same initial MO concentration. When Degussa P25 TiO_2 nanoparticles were used, the initial MO degradation rate was ∼1.203 mg/(g·min). The initial MO degradation rate by the bare Cu_2O nanospheres after the solvent-thermal process increased to ∼3.12 mg/(g·min), ∼259% as that of Degussa P25 TiO_2 nanoparticles. The initial MO degradation rate by these Cu_2O-NS/TiO_2−NI photocatalysts largely increased to ∼12.825 mg/(g·min), ∼1066% as that of Degussa P25 TiO_2 nanoparticles and ∼411% as that of the bare Cu_2O nanospheres after the solvent-thermal process. The largely enhanced photocatalytic degradation effect of these Cu_2O-NS/TiO_2-NI photocatalysts was in accordance with the surface photovoltage spectrum measurement results in Figure 6b.

The stability of a photocatalyst is vital for its potential applications in environmental remediation practice. Figure 7b shows the photocatalytic degradation of MO by these Cu_2O-NS/TiO_2-NI photocatalysts under visible light illumination for seven runs. After one run, the photocatalyst was collected, washed, dried, and then reused in the photocatalytic degradation of MO for the next run. These Cu_2O-NS/TiO_2-

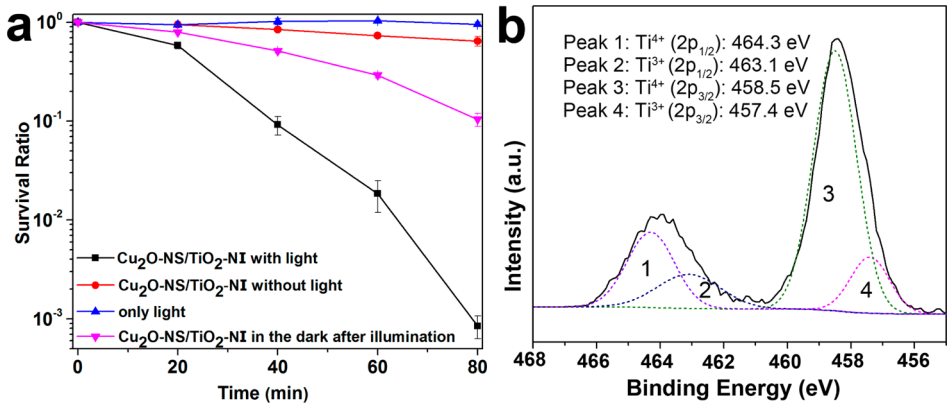

Figure 8. (a) The survival ratio of *E. coli* with the treatment by Cu_2O-NS/TiO_2−NI under visible light illumination, compared with that without photocatalyst under visible light illumination, with photocatalyst in the dark, and with photocatalyst in the dark after illuminated for 3 h first. (b) The high resolution XPS scans over Ti 2p peaks under visible light illumination.

NI photocatalysts demonstrated similar photocatalytic degradation behavior on MO under visible light illumination for the seven runs in general. The residual MO percentage was ∼4% after 40 min treatment and no obvious reduction of the photocatalytic degradation efficiency was observed, which demonstrated that these Cu_2O-NS/TiO_2-NI photocatalysts were stable during the photocatalytic process. It had been reported that Cu_2O nanoparticles were oxidized to CuO during the photocatalytic process as demonstrated by their XRD pattern change and deactivated by photocorrsion.[10,32] Figure 7c compares the XRD patterns of these Cu_2O-NS/TiO_2-NI photocatalysts before and after the MO photocatalytic degradation for seven runs. It clearly demonstrated that their XRD patterns were identical and all peaks still belonged to the fcc Cu_2O phase. Figure 7d shows the HRTEM observation of the sample after the MO photocatalytic degradation for seven runs. Only Cu_2O and TiO_2 lattices could be observed, while no CuO was found on this sample. The XRD and HRTEM results confirmed the good stability of these Cu_2O-NS/TiO_2-NI photocatalysts, which was beneficial to their potential applications. Further stability evidences from the XPS analysis and the diffuse reflectance spectra measurement could be found in Figure S1 and Figure S2, respectively, in the Supporting Information.

3.6. Photocatalytic Disinfection of *Escherichia coli* Bacteria under Visible Light Illumination and Post-illumination Catalytic Memory Disinfection of *Escherichia coli* Bacteria in the Dark. The superior photocatalytic performance of these Cu_2O-NS/TiO_2-NI photocatalysts was further demonstrated by their photocatalytic disinfection effect on the viability of *E. coli* cells, which was conducted by exposing the cells suspended in buffer solution with the photocatalyst under visible light illumination (λ > 400 nm) for varying time intervals. The survival ratio of *E. coli* was determined by the ratio of N_t/N_0, where N_0 and N_t are the numbers of colony-forming units at the initial and each following time interval, respectively. Figure 8 shows the survival ratio of *E. coli* with the treatment by these Cu_2O-NS/TiO_2-NI photocatalysts under visible light illumination, compared with that without photocatalyst under visible light illumination and that with photocatalyst in the dark. When there was no photocatalyst presence, no obvious *E. coli* disinfection was observed under visible light illumination. Without light illumination, these Cu_2O-NS/TiO_2-NI photocatalysts only showed a modest bactericidal effect on *E. coli*. After 80 min treatment, the survival ratio of *E. coli* was still ∼64 %, which should come from the well-known bactericidal effect of copper-based oxides. Under visible light illumination, however, these Cu_2O-NS/TiO_2-NI photocatalysts demonstrated a much better bactericidal effect on *E. coli*. The survival ratio of *E. coli* continuously decreased with the increase of the treatment time. After 80 min treatment, the survival ratio of E. coli dropped to less than 10^{-3}, which was about 3 magnitudes lower than that without visible light illumination. From the comparison, it is clear that their demonstrated superior bactericidal effect on *E. coli* under visible light illumination could be mainly attributed to the superior photocatalytic performance of these Cu_2O-NS/TiO_2-NI photocatalysts, not the modest bactericidal effect from the Cu_2O component itself in this composite photocatalyst system.

Most interestingly, these Cu_2O-NS/TiO_2-NI photocatlysts also demonstrated a post-illumination catalytic memory disinfection of *E. coli* bacteria in the dark. In this experiment, the photocatalyst sample was firstly illuminated by the same lamp used in the photocatalytic disinfection for ∼3 h. Then, the lamp was shut off and the sample was used to conduct disinfection experiments on fresh *E. coli* bacteria in the dark under the same experimental set-up as the photocatalytic disinfection experiment described above, only without the light illumination. The *E. coli* survive ratio curve is shown in Figure 8, which demonstrated clearly that these Cu_2O-NS/TiO_2-NI photocatalysts could effectively disinfect *E. coli* cells in the dark even after the visible illumination was shut off. After 80 min treatment, the survival ratio of *E. coli* dropped to just ∼10%, which was significantly lower than that treated by the same photocatalyst in the dark without pre-illumination. Another disinfection experiment was conducted in the dark with the photocatalyst sample being kept in the dark for 8 h after the visible light illumination was shut off. The survival ratio curve of *E. coli* in this experiment was very close to that treated by the same photocatalyst in the dark without pre-illumination (not shown in Figure 8a). The observed disinfection effect in the dark with pre-illumination was very similar to our previous work on palladium oxide modified nitrogen-doped titanium oxide (TiON/PdO) photocatalyst,[33,34] which could also be attributed to the electron trapping and release occurring when the visible light illumination was on and off, respectively. Figure 8b shows the high resolution XPS scans over Ti 2p peaks under visible light illumination. It could be found that part of Ti^{4+} was reduced to Ti^{3+}, which came from the transfer of photoexcited electrons from Cu_2O to TiO_2 under visible light illumination

dx.doi.org/10.1021/am500131b | ACS Appl. Mater. Interfaces 2014, 6, 5629−5639

and the subsequent trapping of part of these electrons by TiO_2 nanoislands. After the light illumination was shut off, these trapped electrons could be gradually released from TiO_2 to react with O_2 to produce reactive radicals,[35,36] which resulted in this post-illumination catalytic memory disinfection of *E. coli* bacteria in the dark.

3.7. Mechanism on the Enhancement of Photocatalytic Activity and Stability, and Post-illumination Catalytic Memory of Cu_2O Nanospheres Decorated with TiO_2 Nanoislands. Figure 9 shows the proposed energy band

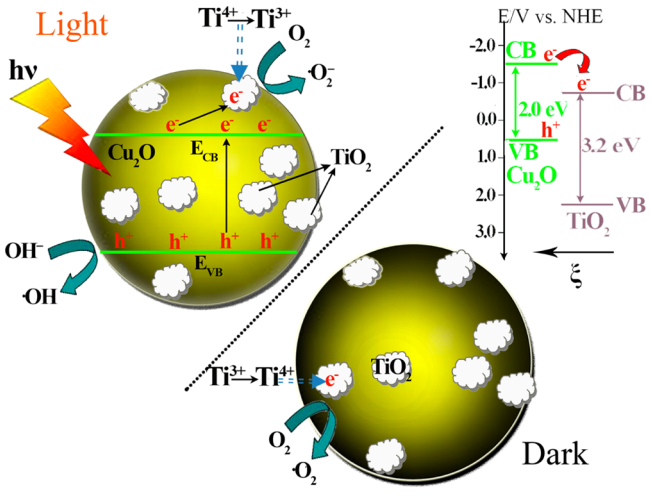

Figure 9. Proposed energy band structure of the Cu_2O/TiO_2 $p-n$ heterojunction, the photocatalytic activity enhancement mechanism under visible light illumination, and the post-illumination catalytic memory mechanism in the dark.

structure of the Cu_2O/TiO_2 $p-n$ heterojunction, the photocatalytic activity enhancement mechanism under visible light illumination,[37,38] and the post-illumination catalytic memory mechanism in the dark. When p-type Cu_2O and n-type TiO_2 formed a heterojunction, charge carrier concentration gradient existed at the interface, which induced the diffusion of electrons from TiO_2 to Cu_2O and the diffusion of holes with the opposite direction until the equilibrium was reached. Thus, an inner electric field (ξ) was built at the interface as Figure 9 showed, which could affect the charge carrier transfer during the photocatalytic process. When the sample was illuminated under visible light ($\lambda > 400$ nm), only Cu_2O was excited to produce electron-hole pairs and the previously established equilibrium could not be kept. Because the conduction band (CB) of Cu_2O is located above the CB of TiO_2, the photogenerated electrons by Cu_2O should be injected into the CB of TiO_2 from the CB of Cu_2O due to the band potential difference. In the meantime, the inner electrostatic field ξ in the heterojunction also provided the driving force for the photogenerated electrons to move from Cu_2O to TiO_2 through the heterojunction.

Thus, both the band potential difference and the electrostatic field ξ in the interface favored the electron transfer from the CB of Cu_2O to that of TiO_2, which effectively separated the electron-hole pairs as the SPS analysis demonstrated in Figure 6b. These separated electrons on TiO_2 could be easily trapped by O_2 to produce superoxide radicals ($^{\bullet}O_2^-$), while holes on Cu_2O could react with water to produce hydroxyl radicals ($\cdot$OH). The radical production could be expressed by reactions 3–6 as follows:[37]

$$Cu_2O + h\nu(\text{vis}) \rightarrow e^- + h^+ \quad (3)$$

$$h^+ + H_2O \rightarrow {}^{\bullet}OH + H^+ \quad (4)$$

$$h^+ + OH^- \rightarrow {}^{\bullet}OH \quad (5)$$

$$e^- + O_2 \rightarrow {}^{\bullet}O_2^- \quad (6)$$

Both $^{\bullet}OH$ and $^{\bullet}O_2^-$ radicals are highly reactive and could effectively degrade organic pollutants like MO,[39,40] and disinfect microorganisms like *E. coli*.[33,34] Thus, a largely enhanced photocatalytic performance was observed on these Cu_2O-NS/TiO_2-NI photocatalysts, compared with pure Cu_2O nanospheres. The design of a partial coverage of TiO_2 nanoislands on Cu_2O nanosphere surface made it possible for photo-generated holes to react with water to produce $\cdot$OHs or directly react with organic pollutants/microorganisms in water. Thus, it could minimize the accumulation of holes on the underlying Cu_2O films or Cu_2O cores for photocorrosion, and subsequently make these Cu_2O-NS/TiO_2-NI photocatalysts stable during the photocatalysis process.

The biological inactivation ability of Cu/TiO_2 photocatalyst system in the dark had been reported by K. Hashimoto et al.[14,41] and S. Rtimi et al.,[15,42] in which they attributed the observed antimicrobial activity in the dark to Cu^+ in the solid-state Cu_xO nanoclusters. In our Cu_2O-NS/TiO_2-NI photocatalyst system, however, the observed *E. coli* disinfection in the dark could not be attributed to the antimicrobial activity of Cu^+. The main component of our Cu_2O-NS/TiO_2-NI photocatalyst was Cu_2O nanospheres. If this disinfection effect in the dark was due to Cu^+, the survival ratio of *E. coli* should be similar no matter there was a pre-illumination or not. However, the survival ratio of *E. coli* in the dark treated by the Cu_2O-NS/TiO_2-NI photocatalyst with the pre-illumination was just ~15% as that without the pre-illumination (see Figure 8a). Furthermore, this catalytic memory effect disappeared after the photocatalyst sample was kept in the dark for 8 h before it was used for the dark disinfection experiment. These observations clearly suggested that other factors contributed to the observed *E. coli* disinfection capability of our Cu_2O-NS/TiO_2-NI photocatalyst in the dark.

The high resolution XPS scans over Ti 2p peaks (see Figure 8b) in our Cu_2O-NS/TiO_2-NI photocatalyst showed that part of Ti^{4+} was reduced to Ti^{3+}, which suggested that electrons generated by Cu_2O must flow to TiO_2 and be trapped there under visible light illumination. After the light illumination was shut off, these trapped electrons could be gradually released from TiO_2 to react with O_2 to produce reactive radicals, which imparted the catalytic memory to our Cu_2O-NS/TiO_2-NI photocatalyst. In our previous work, noble metal oxide PdO was used in TiON/PdO photocatalyst to trap and release photogenerated electrons for its catalytic memory.[33,34] For these Cu_2O-NS/TiO_2-NI photocatalysts, however, no noble metal component was needed to obtain the catalytic "memory". Thus, the material cost could be largely reduced, beneficial for their potential applications. Similar observation had been reported by the research group led by Prof. A. Fujishima on the TiO_2/WO_3 system,[43,44] although they did not name it as the post-illumination catalytic memory effect. They observed that the TiO_2/WO_3 system was active after the UV light illumination was shut off, which was attributed to the trapping and release by WO_3 of photogenerated electrons from TiO_2. Thus, the catalytic memory effect may be possessed by any photocatalyst system, if in which photoexcited electrons could

dx.doi.org/10.1021/am500131b | ACS Appl. Mater. Interfaces 2014, 6, 5629–5639

transfer from the light absorber component to the decoration component while the decoration component could trap and release them.

4. CONCLUSIONS

In summary, Cu_2O nanospheres decorated with TiO_2 nanoislands were synthesized by a facile hydrolyzation reaction followed by a solvent-thermal process. In this Cu_2O/TiO_2 composite photocatalyst, Cu_2O served as the main visible light absorber, while TiO_2 nanoislands formed heterojunctions of good contact with Cu_2O nanospheres for an efficient charge carrier separation and a subsequent increase of the lifetime of the charge carriers. Compared with pure Cu_2O nanospheres without decorated TiO_2 nanoislands, they not only demonstrated a superior photocatalytic performance under visible light illumination for MO degradation and *E. coli* bacteria disinfection, but also possessed a better stability during the photocatalysis process from their specific structure. Part of photoexcited electrons transferred from Cu_2O to TiO_2 was trapped by TiO_2 nanoislands under visible light illumination and then was released in the dark, which could give a catalytic memory to this photocatalyst for producing radicals without light illumination. These Cu_2O nanospheres decorated with TiO_2 nanoislands are promising in a broad range of environmental applications.

■ ASSOCIATED CONTENT

Supporting Information

High resolution XPS scans over Cu $2p_{3/2}$ peak of Cu_2O-NS/TiO_2-NI photocatalyst after its photocatalytic degradation of MO and diffuse reflectance spectra of Cu_2O-NS/TiO_2-NI photocatalyst before and after its photocatalytic degradation of MO. This material is available free of charge via the Internet at http://pubs.acs.org.

■ AUTHOR INFORMATION

Corresponding Author

*E-mail: qili@imr.ac.cn. Phone: +86-24-83978028. Fax: +86-24-23971215.

Notes

The authors declare no competing financial interest.

■ ACKNOWLEDGMENTS

The authors would like to thank Prof. Dejun Wang of College of Chemistry, Jilin University for the experimental assistance on the surface photovoltage spectrum measurement, Mr. Xiangrong Ying of Solid Atomic Imaging Division, Shenyang National Laboratory for Materials Science, Institute of Metal Research, Chinese Academy of Sciences for the experimental assistance on the TEM observation and analysis, and Ms. Mian Song and Ms. Shuang Jiao of Environment Functional Materials Division, Shenyang National Laboratory for Materials Science, Institute of Metal Research, Chinese Academy of Sciences for the experimental assistance on *E. coli* culture. This study was supported by the National Natural Science Foundation of China (Grant No. 51102246), the Knowledge Innovation Program of Institute of Metal Research, Chinese Academy of Sciences (Grant No. Y0N5A111A1), the Youth Innovation Promotion Association, Chinese Academy of Sciences (Grant No.Y2N5711171), and the Scientific Research Foundation for the Returned Overseas Chinese Scholars, State Education Ministry, P. R. China.

■ REFERENCES

(1) Hara, M.; Kondo, T.; Komoda, M.; Ikeda, S.; N. Kondo, J.; Domen, K.; Shinohara, K.; Tanaka, A. Cu_2O as A Photocatalyst for Overall Water Splitting under Visible Light Irradiation. *Chem. Commun.* **1998**, 357−358.

(2) Rai, B. P. Cu_2O Solar Cells: A Review. *Sol. Cells* **1988**, *25*, 265−272.

(3) Musa, A. O.; Akomolafe, T.; Carter, M. J. Production of Cuprous Oxide, A Solar Cell Material, by Thermal Oxidation and A Study of Its Physical and Electrical Properties. *Sol. Energy Mater. Sol. C* **1998**, *51*, 305−316.

(4) Zhang, J.; Liu, J.; Peng, Q.; Wang, X.; Li, Y. Nearly Monodisperse Cu_2O and CuO Nanospheres: Preparation and Applications for Sensitive Gas Sensors. *Chem. Mater.* **2006**, *18*, 867−871.

(5) Wood, B. J.; Wise, H.; Yolles, R. S. Selectivity and Stoichiometry of Copper Oxide in Propylene Oxidation. *J. Catal.* **1969**, *15*, 355−362.

(6) Li, J.; Liu, L.; Yu, Y.; Tang, Y.; Li, H.; Du, F. Preparation of Highly Photocatalytic Active Nano-size TiO_2−Cu_2O Particle Composites with A Novel Electrochemical Method. *Electrochem. Commun.* **2004**, *6*, 940−943.

(7) Zhang, Y.; Deng, B.; Zhang, T. R.; Gao, D. M.; Xu, A. W. Shape Effects of Cu_2O Polyhedral Microcrystals on Photocatalytic Activity. *J. Phys. Chem. C* **2010**, *114*, 5073−5079.

(8) Zhang, X.; Song, J.; Jiao, J.; Mei, X. Preparation and Photocatalytic Activity of Cuprous Oxides. *Solid State Sci.* **2010**, *12*, 1215−1219.

(9) Ho, J. Y.; Huang, M. H. Synthesis of Submicrometer-Sized Cu_2O Crystals with Morphological Evolution from Cubic to Hexapod Structures and Their Comparative Photocatalytic Activity. *J. Phys. Chem. C* **2009**, *113*, 14159−14164.

(10) Huang, L.; Peng, F.; Yu, H.; Wang, H. Preparation of Cuprous Oxides with Different Sizes and Their Behaviors of Adsorption, Visible-Light Driven Photocatalysis and Photocorrosion. *Solid State Sci.* **2009**, *11*, 129−138.

(11) Zheng, Z.; Huang, B.; Wang, Z.; Guo, M.; Qin, X.; Zhang, X.; Wang, P.; Dai, Y. Crystal Faces of Cu_2O and Their Stabilities in Photocatalytic Reactions. *J. Phys. Chem. C* **2009**, *113*, 14448−14453.

(12) Zhang, Y.-G.; Ma, L.-L.; Li, J.-L.; Yu, Y. In Situ Fenton Reagent Generated from TiO_2/Cu_2O Composite Film: ANew Way to Utilize TiO_2 under Visible Light Irradiation. *Environ. Sci. Technol.* **2007**, *41*, 6264−6269.

(13) Huang, L.; Peng, F.; Wang, H.; Yu, H.; Li, Z. Preparation and Characterization of Cu_2O/TiO_2 Nano−Nano Heterostructure Photocatalysts. *Catal. Commun.* **2009**, *10*, 1839−1843.

(14) Qiu, X.; Miyauchi, M.; Sunada, K.; Minoshima, M.; Liu, M.; Lu, Y.; Li, D.; Shimodaira, Y.; Hosogi, Y.; Kuroda, Y.; Hashimoto, K. Hybrid Cu_xO/TiO_2 Nanocomposites As Risk-Reduction Materials in Indoor Environments. *ACS Nano* **2011**, *6*, 1609−1618.

(15) Baghriche, O.; Rtimi, S.; Pulgarin, C.; Sanjines, R.; Kiwi, J. Innovative TiO_2/Cu Nanosurfaces Inactivating Bacteria in the Minute Range under Low-Intensity Actinic Light. *ACS Appl. Mater. Interfaces* **2012**, *4*, 5234−5240.

(16) Lalitha, K.; Sadanandam, G.; Kumari, V. D.; Subrahmanyam, M.; Sreedhar, B.; Hebalkar, N. Y. Highly Stabilized and Finely Dispersed Cu_2O/TiO_2: A Promising Visible Sensitive Photocatalyst for Continuous Production of Hydrogen from Glycerol:Water Mixtures. *J. Phys. Chem. C* **2010**, *114*, 22181−22189.

(17) Chu, S.; Zheng, X.; Kong, F.; Wu, G.; Luo, L.; Guo, Y.; Liu, H.; Wang, Y.; Yu, H.; Zou, Z. Architecture of Cu_2O@TiO_2 Core−Shell Heterojunction and Photodegradation for 4-nitrophenol under Simulated Sunlight Irradiation. *Mater. Chem. Phys.* **2011**, *129*, 1184−1188.

(18) Paracchino, A.; Mathews, N.; Hisatomi, T.; Stefik, M.; Tilley, S. D.; Grätzel, M. Ultrathin Films on Copper(I) Oxide Water Splitting Photocathodes: A Study on Performance and Stability. *Energy Environ. Sci.* **2012**, *5*, 8673.

(19) Yec, C. C.; Zeng, H. C. Synthetic Architecture of Multiple Core−Shell and Yolk−Shell Structures of $(Cu_2O@)nCu_2O$ (n = 1−4) with Centricity and Eccentricity. *Chem. Mater.* **2012**, *24*, 1917−1929.

(20) Yanhong, L.; Dejun, W.; Qidong, Z.; Min, Y.; Qinglin, Z. A Study of Quantum Confinement Properties of Photogenerated Charges in ZnO Nanoparticles by Surface Photovoltage Spectroscopy. *J. Phys. Chem. B* **2004**, *108*, 3202−3206.
(21) Barret, C. S. *Structure of Metals*; McGraw-Hill: New York, 1966.
(22) Teo, J. J.; Chang, Y.; Zeng, H. C. Fabrications of Hollow Nanocubes of Cu_2O and Cu via Reductive Self-Assembly of CuO Nanocrystals. *Langmuir* **2006**, *22*, 7369−77.
(23) Poulston, S.; Parlett, P. M.; Stone, P.; Bowker, M. Surface Oxidation and Reduction of CuO and Cu_2O Studied Using XPS and XAES. *Surf. Interface Anal.* **1996**, *24*, 811−820.
(24) Yin, M.; Wu, C.-K.; Lou, Y.; Burda, C.; Koberstein, J. T.; Zhu, Y.; O'Brien, S. Copper Oxide Nanocrystals. *J. Am. Chem. Soc.* **2005**, *127*, 9506−9511.
(25) Ghijsen, J.; Tjeng, L. H.; van Elp, J.; Eskes, H.; Westerink, J.; Sawatzky, G. A.; Czyzyk, M. T. Electronic Structure of Cu_2O and CuO. *Phys. Rev. B* **1988**, *38*, 11322−11330.
(26) Balamurugan, B.; Mehta, B. R.; Shivaprasad, S. M. Surface-Modified CuO Layer in Size-Stabilized Single-Phase Cu_2O Nanoparticles. *Appl. Phys. Lett.* **2001**, *79*, 3176−3178.
(27) Tauc, J.; Grigorovici, R.; Vancu, A. Optical Properties and Electronic Structure of Amorphous Germanium. *Phys. Status Solidi B* **1966**, *15*, 627−637.
(28) de Jongh, P. E.; Vanmaekelbergh, D.; Kelly, J. J. Cu_2O: Electrodeposition and Characterization. *Chem. Mater.* **1999**, *11*, 3512−3517.
(29) Kronik, L.; Shapira, Y. Surface Photovoltage Phenomena: Theory, Experiment, and Applications. *Surf. Sci. Rep.* **1999**, *37*, 1−206.
(30) Duzhko, V.; Timoshenko, V. Y.; Koch, F.; Dittrich, T. Photovoltage in Nanocrystalline Porous TiO_2. *Phys. Rev. B* **2001**, *64*, No. 075204.
(31) Xu, H.; Wang, W.; Zhu, W. Shape Evolution and Size-Controllable Synthesis of Cu_2O Octahedra and Their Morphology-Dependent Photocatalytic Properties. *J. Phys. Chem. B* **2006**, *110*, 13829−13834.
(32) Bessekhouad, Y.; Robert, D.; Weber, J. V. Photocatalytic Activity of Cu_2O/TiO_2, Bi_2O_3/TiO_2 and $ZnMn_2O_4/TiO_2$ Heterojunctions. *Catal. Today* **2005**, *101*, 315−321.
(33) Li, Q.; Li, Y. W.; Wu, P.; Xie, R.; Shang, J. K. Palladium Oxide Nanoparticles on Nitrogen-Doped Titanium Oxide: Accelerated Photocatalytic Disinfection and Post-Illumination Catalytic "Memory. *Adv. Mater.* **2008**, *20*, 3717−3723.
(34) Li, Q.; Li, Y. W.; Liu, Z.; Xie, R.; Shang, J. K. Memory Antibacterial Effect from Photoelectron Transfer between Nanoparticles and Visible Light Photocatalyst. *J. Mater. Chem.* **2010**, *20*, 1068−1072.
(35) Nakaoka, Y.; Nosaka, Y. ESR Investigation into the Effects of Heat Treatment and Crystal Structure on Radicals Produced over Irradiated TiO_2 Powder. *J. Photochem. Photobiol. A* **1997**, *110*, 299−305.
(36) Li, F. B.; Li, X. Z. The Enhancement of Photodegradation Efficiency using Pt−TiO_2 Catalyst. *Chemosphere* **2002**, *48*, 1103−1111.
(37) Yang, L.; Luo, S.; Li, Y.; Xiao, Y.; Kang, Q.; Cai, Q. High Efficient Photocatalytic Degradation of *p*-Nitrophenol on a Unique Cu_2O/TiO_2 *p*−*n* Heterojunction Network Catalyst. *Environ. Sci. Technol.* **2010**, *44*, 7641−7646.
(38) Hou, Y.; Li, X. Y.; Zhao, Q. D.; Quan, X.; Chen, G. H. Fabrication of Cu_2O/TiO_2 Nanotube Heterojunction Arrays and Investigation of Its Photoelectrochemical Behavior. *Appl. Phys. Lett.* **2009**, *95*, No. 093108.
(39) Yan, S. C.; Li, Z. S.; Zou, Z. G. Photodegradation of Rhodamine B and Methyl Orange over Boron-doped g-C_3N_4 under Visible Light Irradiation. *Langmuir* **2010**, *26*, 3894−901.
(40) Chen, F.; Deng, Z.; Li, X.; Zhang, J.; Zhao, J. Visible Light Detoxification by 2,9,16,23-Ttetracarboxyl Phthalocyanine Copper Modified Amorphous Titania. *Chem. Phys. Lett.* **2005**, *415*, 85−88.
(41) Irie, H.; Miura, S.; Kamiya, K.; Hashimoto, K. Efficient Visible Light Sensitive Photocatalysts: Grafting Cu(II) Ions onto TiO_2 and WO_3 Photocatalysts. *Chem. Phys. Lett.* **2008**, *457*, 202−205.
(42) Baghriche, O.; Rtimi, S.; Pulgarin, C.; Sanjines, R.; Kiwi, J. Effect of the Spectral Properties of TiO_2, Cu, TiO_2/Cu Sputtered Films on the Bacterial Inactivation under Low Intensity Actinic Light. *J. Photochem. Photobiol. A* **2013**, *251*, 50−56.
(43) Tatsuma, T.; Takeda, S.; Saitoh, S.; Ohko, Y.; Fujishima, A. Bactericidal Effect of An Energy Storage TiO_2−WO_3 Photocatalyst in Dark. *Electrochem. Commun.* **2003**, *5*, 793−796.
(44) Ngaotrakanwiwat, P.; Tatsuma, T.; Saitoh, S.; Ohko, Y.; Fujishima, A. Charge−Discharge Behavior of TiO_2−WO_3 Photocatalysis Systems with Energy Storage Ability. *Phys. Chem. Chem. Phys.* **2003**, *5*, 3234.